A NUMERICAL STUDY OF THE MAXIMUM SCOUR DEPTH AROUND INCLINED BRIDGE PIERS AND COMPARISON WITH AN EXPERIMENTAL MODEL

GHASEMI ASL M.[1], HEIDARNEJAD M.[2*]

[1] Department of Civil Engineering, Ahvaz Branch, Islamic Azad University, Ahvaz, Iran

[2] Corresponding author: Department of Water Science Engineering, Ahvaz Branch, Islamic Azad University, Ahvaz, Iran

(*) mo_he3197@yahoo.com

ABSTRACT

Local scour holes develop around bridges due to the flow coming into collision with the piers and the resulting flow separation. The scour hole dimensions around bridge piers depend on flow hydrodynamics, fluid properties, pier geometry, and bed-load properties. Accordingly, this study numerically investigates the maximum scour depth around inclined bridge piers using FLOW 3D and compares the results with an experimental model. The maximum vertical flow velocity was found to increase by 50% by increasing the Froude number (Fr) from 0.49 to 0.73. Furthermore, the vertical flow velocity was reduced by 41% on average by increasing the bridge pier inclination from 0 to 15°. The results indicate that increasing the pier inclination from 0 to 15° reduces the average maximum scour depth by 28.2, 21.6, 18.5, and 20% at 12, 14, 16, and 18 l.s⁻¹ flow rates, respectively. The scour is exacerbated by increasing the flow rate. Increasing Fr from 0.49 to 0.73 leads to an average 18% increase in the maximum scour depth. The results are suggestive of a 3.4% difference between the FLOW-3D simulation results and the physical model. The comparison showed the results to be consistent and the FLOW-3D simulation accurate.

Keywords: FLOW 3D, Erosion, Inclined Bridge Pier, Simulation.

INTRODUCTION

Bridges promote scour in their vicinity for several reasons. First, bridge cross-sections are assumed to be smaller than the river section to shorten the bridge, increasing the flow velocity and bed shear stress, which leads to scour (contraction scour). Furthermore, vortex formation around the piers and abutments of three-dimensional systems removes particles from the bed, leading to local scour. This type of scour is particularly notable for the complex flow conditions associated with it. If present in the river, general scour exacerbates the effects of bridge scour. The primary factor behind local bridge pier scour is the downward flow acting as a vertical water jet, lifting the bed material from around bridge piers. The horseshoe vortex system is one consequence of local scour. According to some studies, this system is small and weak in the beginning but grows in size and power after a scour hole is formed. As the scour depth increases, the downward flow near the hole floor deteriorates, halting scour hole development when the driving forces balance out with the resisting forces (saturation weight). Live-bed scour occurs naturally in many rivers. Factors such as nonerodible riverbanks or a bend in the course of the river promote natural riverbed scour as the stream washes the sediments away from the bed and banks on the outside bend and toward the inside (Hasounizadeh, 1991). When the flow velocity or shear exceeds the critical level, the scour depth fluctuates around the equilibrium scour depth due to the transport of sand masses starting upstream. Scour is a real threat to the structural integrity of bridges and hydraulic structures and can eventually lead to foundation failures and bridge collapses (Wardhana and Hadipriono, 2003). Although several studies have focused on explaining the scour mechanism, some aspects of the phenomenon remain unsettled with contradicting claims in the literature. According to Hoffmans and Verheij (1997), scour analysis is an integral part of foundation design for modern bridges and guarantees the robustness of bridges against strong floods. Local scour is a global problem with a devastating risk of casualties. Melville and Coleman (2000) estimated the yearly bridge-scour damage in New Zealand at NZ\$ 36 million. A focused study on bridge failure in the United States by Cheremisinoff, Cheremisinoff, and Cheng (1987) quotes a report from the U.S. Federal Highway Administration, which claims that regional floods have caused approximately \$1 million in damage to bridges and highways each year from 1964 to 1972. The 1989 disaster of the Hatchie River bridge collapse claimed eight lives, and the 1993 North Mississippi flood destroyed 23 bridges, causing an estimated 15\$ million worth of damage. The massive floods caused by the 1994 Tropical Storm Alberto caused scour damage to more than 500 bridges in Georgia, 73 of which required substantial repair. Nearly 86% of the 577,000 bridges in the U.S. National Bridge Registry are built over waterways, and more than 26,000 of those are exposed to severe scour. Overall, approximately 85,000 U.S. bridges are threatened by scour (Richardson and Davies, 1995). Karimi, Heidarnejad and Masjedi (2017) studied the effects of bridge pier inclination on scour on a straight Plexiglas experimental flume. In this study, a cylindrical pier was placed in the stream at four inclinations and four flow rates for clear-water experiments. The flume bed was covered with evenly graded sand. It was shown that the maximum and minimum scour depths corresponded to cases with 0 and 15° pier inclinations. Furthermore, scour hole dimensions were also found to

decrease as the piers were moved in the flow direction. Christian Chreties, Gonzalo Simarro, and Luis Teixeira (2008) adopted a new experimental method to find the equilibrium scour for bridge piers. Assuming that the scour hole shape depends on the scour depth and sediment properties and not the flow conditions, they concluded that the proposed method could help considerably reduce the experimentation time, eliminating any doubts about equilibrium scour. Relying on the Group Method of Data Handling (GMDH), Najafzadeh, Barani, and Hessami-Kermani (2013a) estimated the live-bed scour depth around bridge piers in clear-water experiments. They used an AI-based, self-adaptive, GMDH, numerical model to estimate the scour depth around bridge piers in a live sediment bed under clear-water conditions.

Kazemian et al. (2023) studied bridge pier scour monitoring techniques and advances in vibration-based pier scour monitoring. Drawing on experimental and field analyses, they showed that a structure can be monitored based on scour-induced vibration changes, and affordable and accurate scour monitoring systems can be designed in light of technological advances achieved in the past decade.

Aijun et al. (2020) analyzed the probabilistic seismic responses of coastal highway bridges under scour conditions and hydrodynamic effects. They found that the hydrodynamic effect would be greater at larger scour depths.

In a study on protective measures against bridge pier scour, Chiew (1992) states that the equilibrium scour depth is obtained when the scour depth changes by no more than 1 mm over an eight-hour period. In an experimental study, Bozkus and Çeşme (2010) addressed scour depth reduction by using inclined piers. The clear-water experiments involved two piers with thicknesses of 5 and 7 cm, different flow depths and flow rates, and four inclinations (namely, 0, 5, 10, and 15°). The mean sediment particle size was 1.44 mm with a standard deviation of 3. Through measurement and comparison, the authors decided that increasing the pier inclination can effectively reduce the scour depth.

Thanks to progress in construction technologies, several examples of such bridges have been built around the world. One example is the Ahwaz Eighth Bridge in Iran. Scouring around inclined bridge piers has never been studied before; therefore, a numerical model was used to analyze the problem.

Figure 1: Ahwaz Eighth Bridge, Iran, supported by inclined piers (Karimi et al., 2017)

MATERIALS AND METHODS

The experimental results of Karimi et al. (2017) were used to calibrate the numerical FLOW-3D model, comparing it with the physical model in terms of scour around inclined bridge piers. The flume used in this study was located at the Sediments Laboratory of the Khuzestan Water and Power Organization, Khuzestan Province, Iran.

Figure 2: Experiments with the physical model

FLOW 3D

This software program solves the equations governing fluid motions with a finite-volume approach by dividing the stream into a network of pipe-like cells. Each cell has its dependent variables, that is, all variables are calculated for the center of the cell, except for the velocity, which is calculated at the center of the cell. FLOW 3D relies on two numerical techniques for geometrical simulation.

Volume of Fluid (VOF): This method is used to represent the free-surface fluid behavior.

Fractional Area–Volume Obstacle Representation (FAVOR): This method is used for simulating rigid surfaces and bodies.

The VOF method adopted in FLOW 3D is based on donor–acceptor approximations introduced by Hirt and Nichols (1981). These governing equations are referred to as Navier–Stokes equations. Representing the flow velocity, these equations are based on the balance of forces exerted on a small volume in the laminar flow. Reynolds averaging is then used for conversion into turbulent flow conditions.

This study employed the mass and momentum equations as follows:

$$V_F \frac{\partial \rho}{\partial t} + \frac{\partial}{\partial x}\left(\rho u A_x\right) + R \frac{\partial}{\partial y}\left(\rho v A_y\right) + \frac{\partial}{\partial z}\left(\rho w A_z\right) + \xi \frac{\rho u A_x}{x} = RDIF + RSOR \qquad (1)$$

Bridge Pier Meshing

Given the importance of meshing, a large number of meshing cells were used. However, since increasing the number of cells extends the run time, a trade-off was made between accuracy and run time. It must be noted that cell divisions do not affect streamlines and only serve the meshing process.

Meshing changes in different directions based on the block length. After the meh size is determined, FLOW 3D enables users to verify the accuracy of cell proportions in the *x*, *y*, and *z* directions using the maximum adjacent cell size ratio and maximum aspect ratio. The two parameters can be found under Info in the Meshing tab.
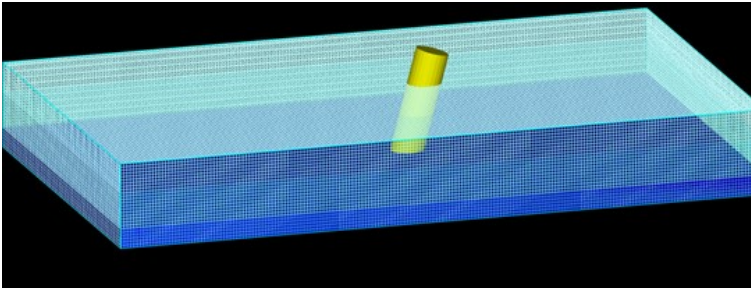
Figure 3: Flume meshing

Boundary Conditions

The boundary conditions are defined under *Boundaries*:

The inflow boundary was of the Volume Flow Rate type: The inflow rate was also determined in this area. Furthermore, the outflow boundary condition was considered for the outlet. The bottom boundary, as well as the boundaries on the left and right, were wall-type, which is used to separate the fluid from solid boundaries. Under this boundary condition, the vertical and tangent velocities are zero on the walls. Furthermore, the symmetry condition was considered on the top wall.

Calibration

Based on the sensitivity analysis results, the following two parameters are used to calibrate the model:

1. Manning's roughness coefficient (n)
2. Turbulence models

The model was calibrated based on experimental measurements and with different roughness coefficients and turbulence models. The experimental details were as follows:

Manning's roughness coefficient (n): 0.02, 0.025, 0.03, 0.035, and 0.04

Notable turbulence models that are commonly used in this program:

Laminar

Prandtl Mixing Length Model

K–ε Model

Inflow rate: 18 l.s^{-1}

Water level in the flume: 5.5 cm

Flow velocity in the flume: 0.54 l.s^{-1}

Each experiment was carried out with a different inflow rate and an outlet water level at one of the calibration parameters. The results of each experiment were used to calculate the flow velocity in the software program, comparing with the experimental value (0.54 m.s^{-1}) and calculating the error.

The simulation run time was set at 7200 seconds in all experiments.

Main Model Experiments

The same experimental variables as in the physical model experiments were considered in the numerical model to allow for estimating the error by a comparison between physical and numerical models. The experiments were carried out at four flow rates (namely, 12, 14, 16, and 18 l.s^{-1}) and four bridge inclinations (0, 5, 10, and 15°). The experimental details are listed in Table 3.

Table 1: Main experiments

Scenario	Depth (cm)	Discharge (L/s)	Velocity (m/s)	Fr	Bridge pier angle
1	5.5	12	0.36	0.49	0
2					5
3					10
4					15
5		14	0.42	0.57	0
6					5
7					10
8					15
9		16	0.48	0.65	0
10					5
11					10
12					15
13		18	0.54	0.73	0
14					5
15					10
16					15

RESULTS

Calibration Results

According to the calibration results, the smallest error in the experiments (*1.45%*) corresponded to the case with the *0.035* Manning's roughness coefficient and the K–ε turbulence model.

Now, the experiments are carried out using the calibration results.

Graphical Results

A three-dimensional view of the four simulated bridges with different inclinations is presented below.
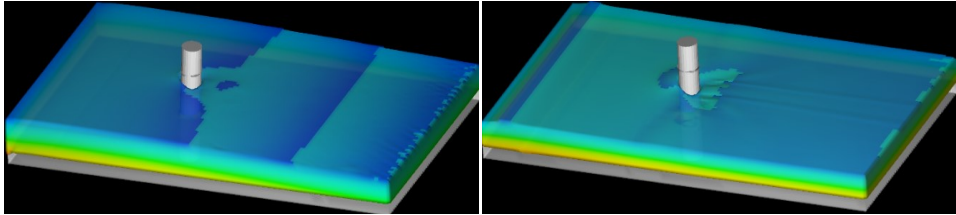

Figure 4: Three-dimensional representation of bridge configurations with 0 and 5° pier inclinations
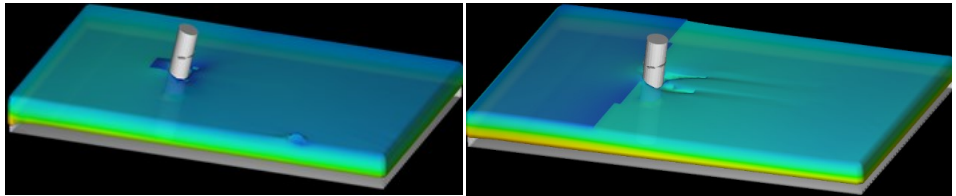
Figure 5: Three-dimensional representation of bridge configurations with 10 and 15° pier inclinations

Flow Velocity Results

Flow velocity results are presented in this section.

It is evident from Figure 6 that increasing Fr from 0.49 to 0.73 increased the maximum vertical flow velocity by 50%. Furthermore, the vertical flow velocity dropped by *41%* on average by increasing the bridge pier inclination from 0 to 15°. Furthermore, according to the graphical representation of the velocity distribution of Figs. 7 to 10, placing the bridge piers in the flume pushed the velocity distribution to the sides of the pier, exacerbating scour in these areas.
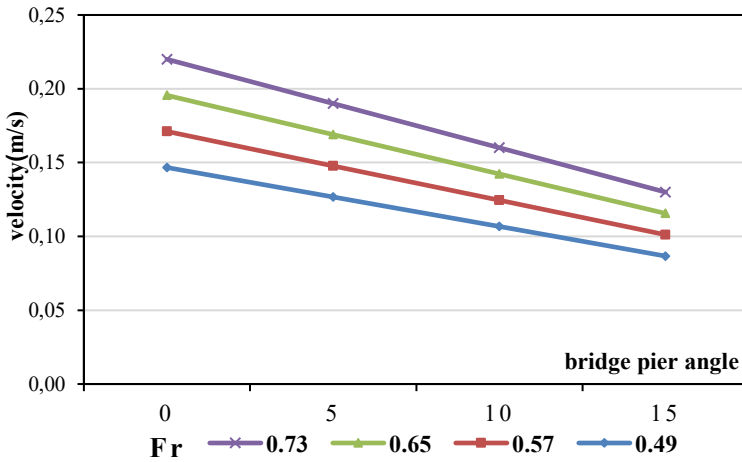
Figure 6: Maximum downward vertical velocity results

Scour Results

Scour Results at a 12 l.s⁻¹ Flow Rate

This section presents scour results at a *12 l.s⁻¹* flow rate and *Fr = 0.49* for all bridge pier inclinations. The results describe sediment transformations both graphically and in the table. The graphical results include the basin plan and the distribution of sediment parameters, including bed deformations, in the computational model.
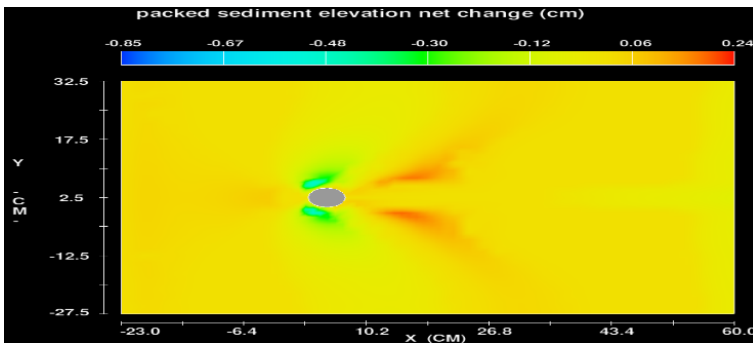

Figure 7: Scour at a 12 l.s⁻¹ flow rate and 0° bridge pier inclination
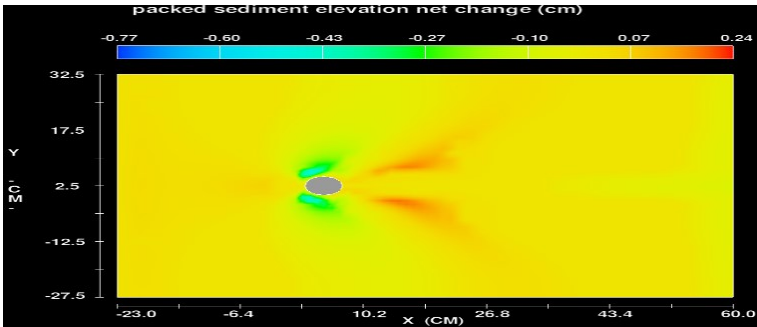
Figure 8: Scour at a 12 l.s⁻¹ flow rate and 5° bridge pier inclination
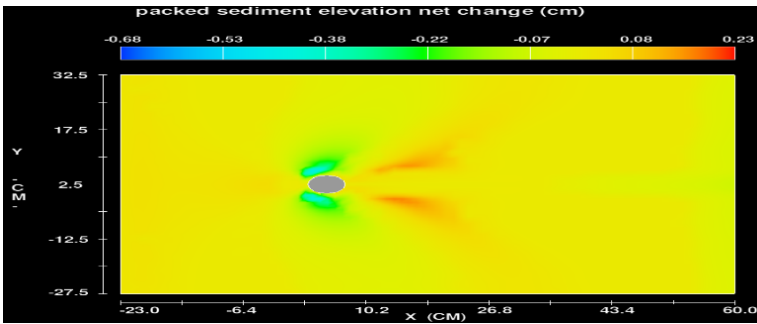
Figure 9: Scour at a 12 l.s⁻¹ flow rate and 10° bridge pier inclination
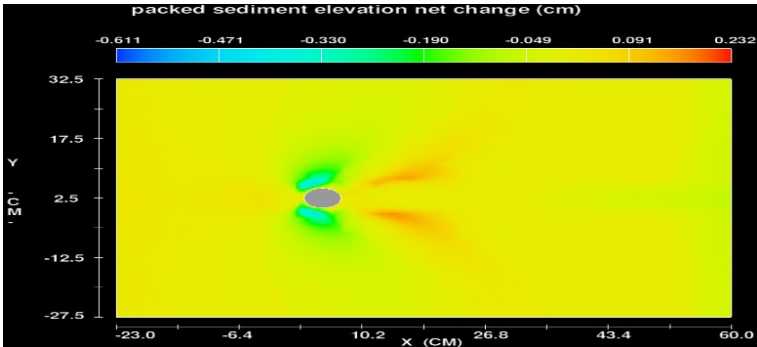
Figure 10: Scour at a 12 l.s⁻¹ flow rate and 15° bridge pier inclination

Table 2: Scour results at 12 l.s⁻¹

scenario	Depth (cm)	Discharge (L/s)	Velocity (m/s)	Fr	Bridge pier angle	Scour depth (ds) (cm)	ds/D
1	5.5	12	0.36	0.49	0	0.85	0.15
2					5	0.77	0.14
3					10	0.68	0.12
4					15	0.61	0.11
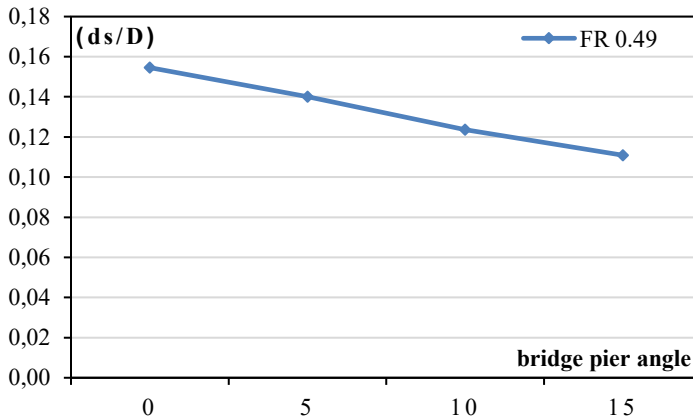
Figure 11: Maximum scour depth at 12 l.s⁻¹

It is evident from the graphical representation of the results in Figs. 7 to 10 that the scour is the strongest around bridge piers due to the higher flow velocity in these parts. Furthermore, according to Table 2 and Figure 11, it is evident that increasing the bridge pier inclination from *0* to *15* reduced the maximum scour depth by *28.2%* on average.

Scour Results at a 14 l.s-1 Flow Rate

This section presents scour results at a *14 l.s⁻¹* flow rate and *Fr = 0.57* for all bridge pier inclinations. The results describe sediment transformations both graphically and in the table. The graphical results include the basin plan and the distribution of sediment parameters, including bed deformations, in the computational model.
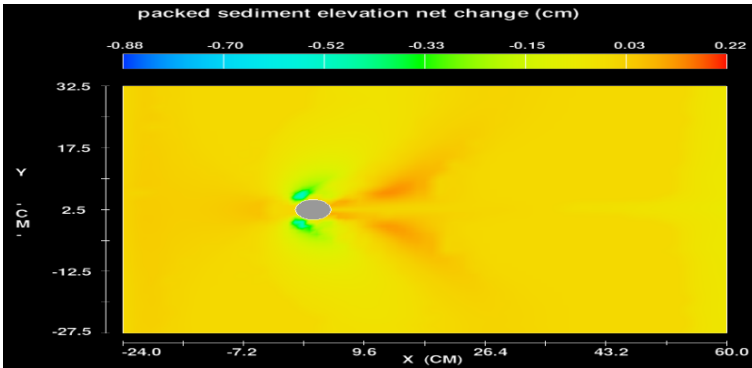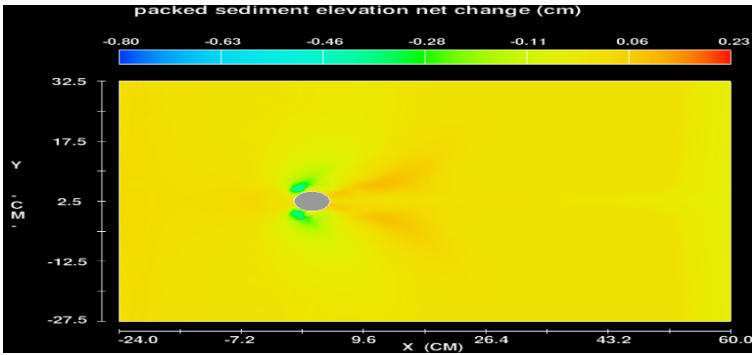
Figure 12: Scour at a 14 l.s^{-1} flow rate and 0° bridge pier inclination

Figure 13: Scour at a 14 l.s^{-1} flow rate and 5° bridge pier inclination
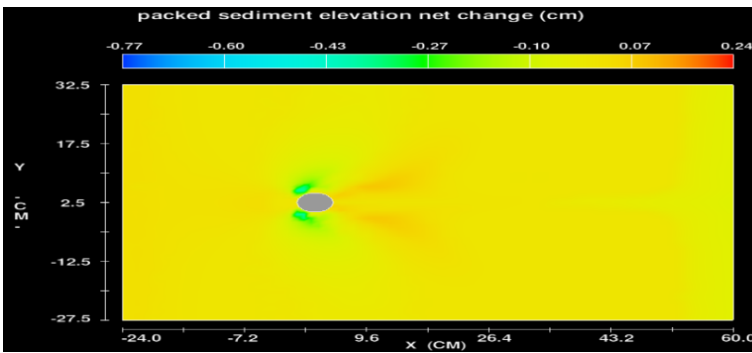

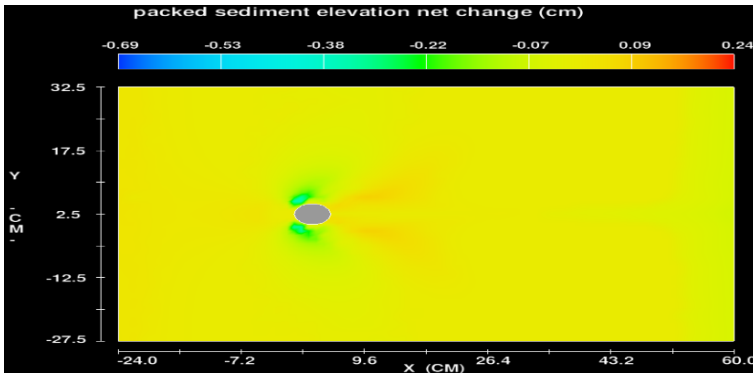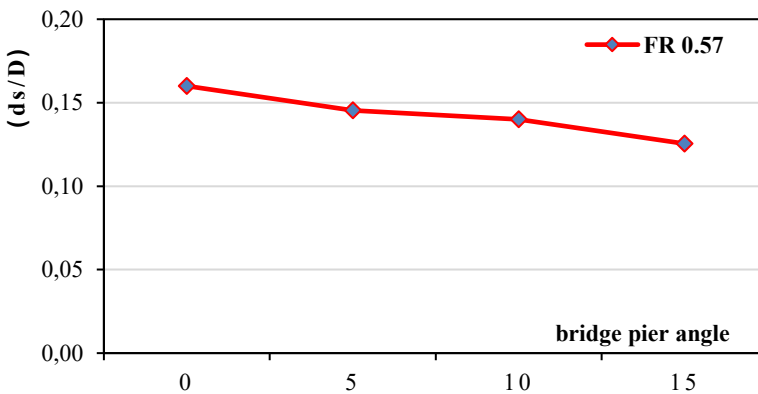**Figure 14: Scour at a 14 l.s^{-1} flow rate and 10° bridge pier inclination**

Figure 15: Scour at a 14 l.s^{-1} flow rate and 15° bridge pier inclination

Table 3: Scour results at 14 l.s^{-1}

Scenario	Depth (cm)	Discharge (L/s)	Velocity (m/s)	Fr	Bridge pier angle	Scour depth (ds) (cm)	ds/D
5	5.5	14	0.42	0.57	0	0.88	0.16
6					5	0.8	0.15
7					10	0.77	0.14
8					15	0.69	0.13

Figure 16: Maximum scour depth at 14 l.s^{-1}

It is evident from the graphical representation of the results in Figs. 12 to 15 that the scour is the strongest around bridge piers due to the higher flow velocity in these parts. Furthermore, according to Table 3 and Figure 16, increasing the bridge pier inclination from 0 to 15 reduced the maximum scour depth by 21.6% on average.

Scour Results at a 16 l.s⁻¹ Flow Rate

Scour Results at a 16 l.s⁻¹ Flow Rate

This section presents scour results at a *16 l.s⁻¹* flow rate and *Fr = 0.65* for all bridge pier inclinations. The results describe sediment transformations both graphically and in the table. The graphical results include the basin plan and the distribution of sediment parameters, including bed deformations, in the computational model.
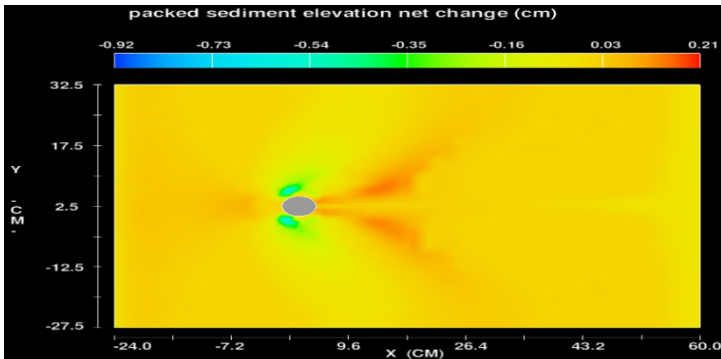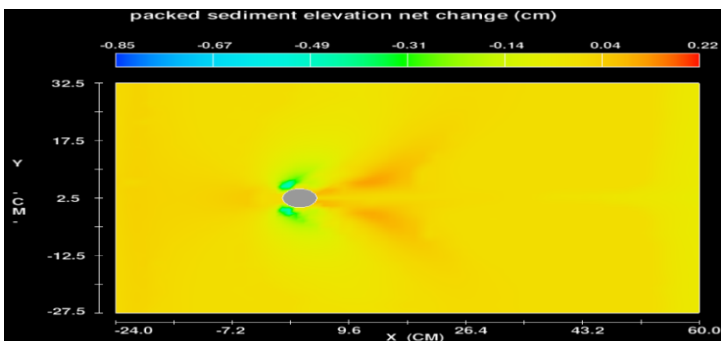

Figure 17: Scour at a 16 l.s⁻¹ flow rate and 0° bridge pier inclination

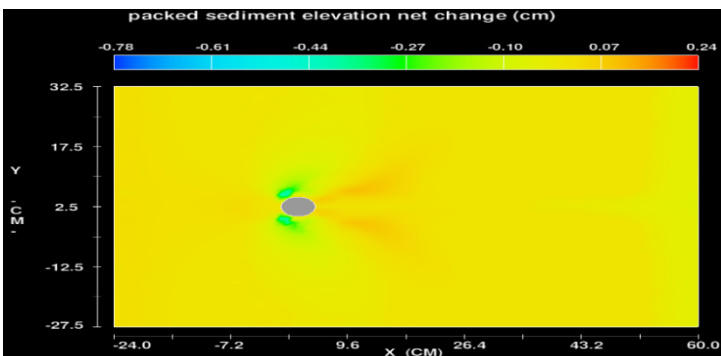**Figure 18: Scour at a 16 l.s⁻¹ flow rate and 5° bridge pier inclination**

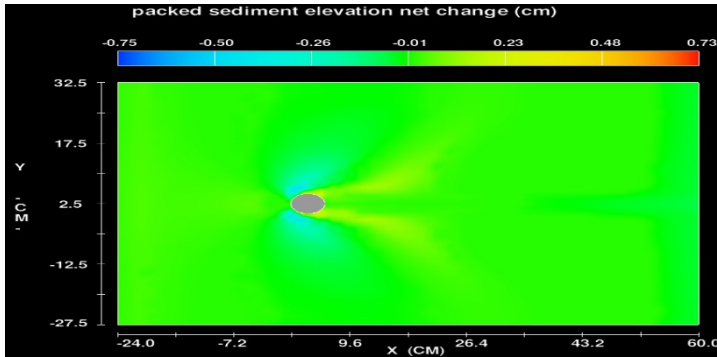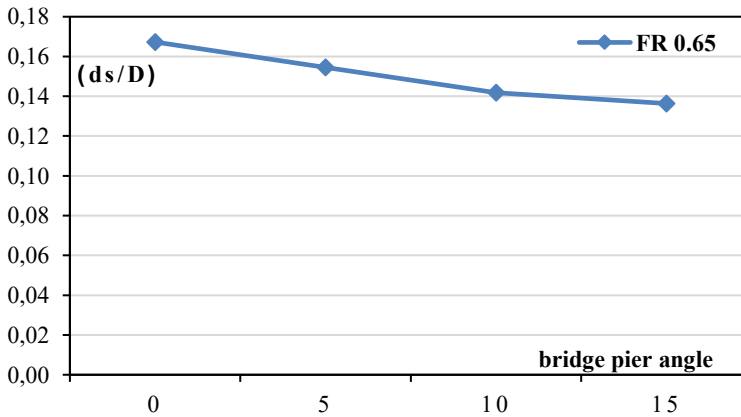**Figure 19: Scour at a 16 l.s⁻¹ flow rate and 10° bridge pier inclination**

Figure 20: Scour at a 16 l.s⁻¹ flow rate and 15° bridge pier inclination

Table 4: Scour results at 16 l.s⁻¹

Scenario	Depth (cm)	Discharge (L/s)	Velocity (m/s)	Fr	Bridge pier angle	Scour depth (ds) (cm)	ds/D
9	5.5	16	0.48	0.65	0	0.92	0.17
10					5	0.85	0.15
11					10	0.78	0.14
12					15	0.75	0.14

Figure 21: Maximum scour depth at 16 l.s⁻¹

It is evident from the graphical representation of the results in Figs. 17 to 20 that the scour is the strongest around bridge piers due to the higher flow velocity in these parts. Furthermore, according to Table 4 and Figure 21, it is clear that increasing the bridge pier inclination from *0* to *15* reduced the maximum scour depth by *18.5%* on average.

Scour Results at an 18 l.s⁻¹ Flow Rate

Scour Results at an 18 l.s^{-1} Flow Rate

This section presents scour results at an 18 l.s^{-1} flow rate and Fr = 0.73 for all bridge pier inclinations. The results describe sediment transformations both graphically and in the table. The graphical results include the basin plan and the distribution of sediment parameters, including bed deformations, in the computational model.
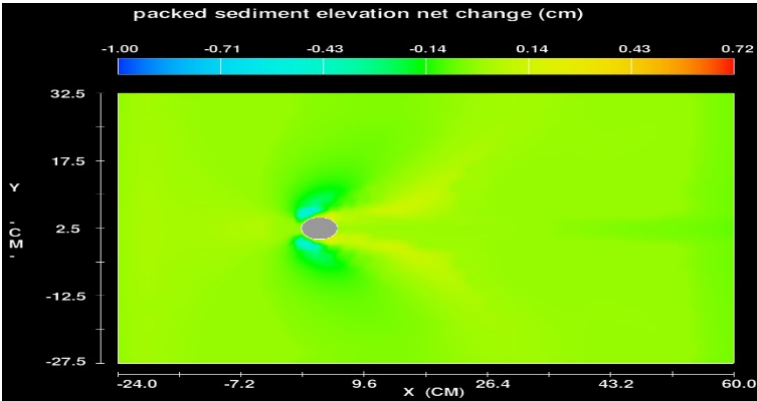
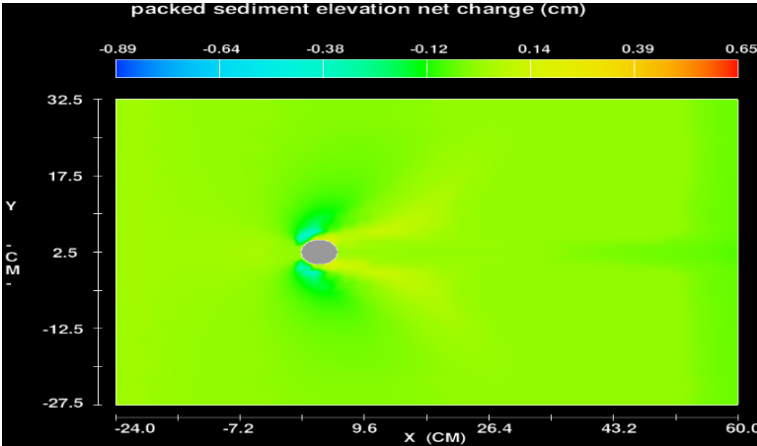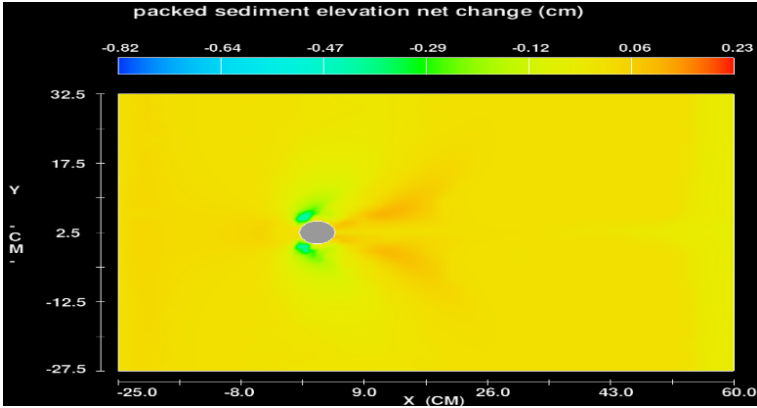**Figure 22: Scour at an 18 l.s^{-1} flow rate and 0° bridge pier inclination**

Figure 23: Scour at an 18 l.s^{-1} flow rate and 5° bridge pier inclination

Figure 24: Scour at an 18 l.s⁻¹ flow rate and 10° bridge pier inclination
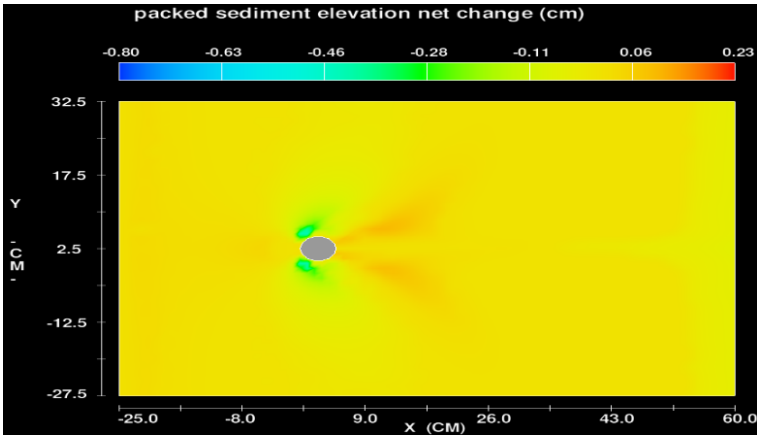

Figure 25: Scour at an 18 l.s⁻¹ flow rate and 15° bridge pier inclination

Table 5: Scour results at 18 l.s⁻¹

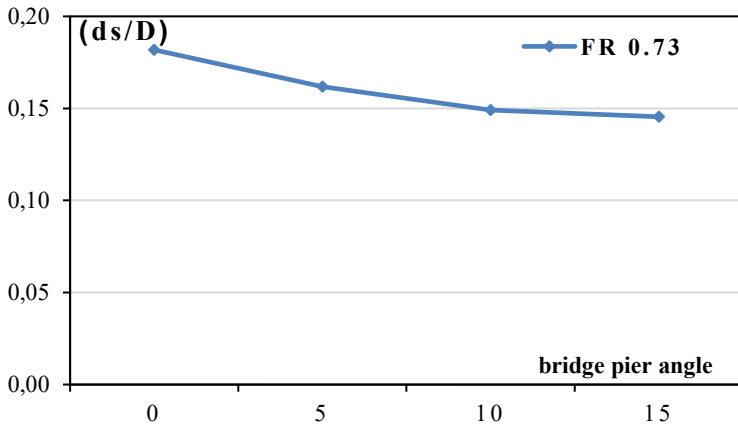| Scenario	Depth (cm)	Discharge (L/s)	Velocity (m/s)	Fr	Bridge pier angle	Scour depth (ds) (cm)	ds/D
13	5.5	18	0.54	0.73	0	1	0.18
14					5	0.89	0.16
15					10	0.82	0.15
16					15	0.8	0.15

Figure 26: Maximum scour depth at 18 l.s⁻¹

It is evident from the graphical representation of the results in Figs. 22 to 25 that the scour is the strongest around bridge piers due to the higher flow velocity in these parts. Furthermore, according to Table 5 and Figure 26, it is evident that increasing the bridge pier inclination from 0 to 15 reduced the maximum scour depth by 20.0% on average.

Effects of Flow Rate on Scour

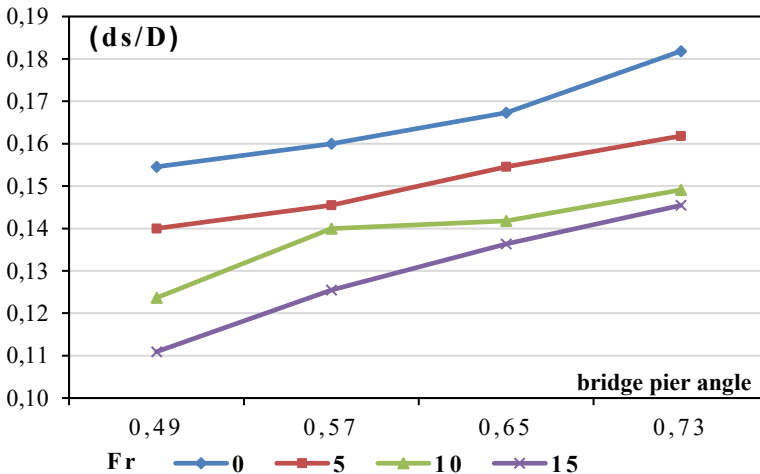In the following, the effects of flow-rate variations on scour are discussed.

Figure 27: The effects of Fr on scour

Figure 27 illustrates that scour is intensified by increasing the flow rate. Raising the Fr from 0.49 to 0.73 led to an a verage 18% increase in the maximum scour depth.

Physical Model Results and FLOW-3D Simulations

In the following, the physical model results are compared with FLOW-3D simulations. In 2015, Karimi et al. studied local scour around inclined bridge piers. Given the similarity of the initial conditions for simulation with the physical model, the simulation results can be verified by comparing the numerical FLOW-3D results with experimental results.
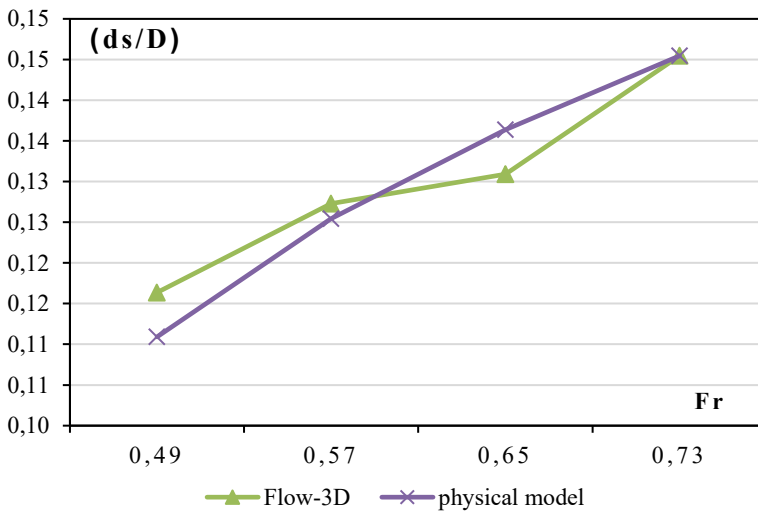

Figure 28: Comparing the FLOW-3D simulation with physical model results

Figure 28 compares the experimental results with the FLOW-3D simulation. According to the control graph, a 3.4% difference appeared between the FLOW-3D simulation and the physical model. The comparison shows how close the results are, proving the accuracy of the FLOW-3D simulation.

CONCLUSION

Increasing Fr from 0.49 to 0.73 was found to increase the maximum vertical flow velocity by 50%. Furthermore, the vertical flow velocity was reduced by 41% on average as a result of increasing the bridge pier inclination from 0 to 15°. A graphical representation of the velocity distribution showed that placing the bridge piers in the flume pushed the velocity distribution to the sides of the pier, exacerbating scour in these areas. Furthermore, investigating the effects of bridge pier inclination on scour (based on the

graphical representation of scour results) shows that scour is the strongest near bridge piers due to the increased velocity in these areas. Moreover, it was found that increasing the pier inclination from 0 to 15° reduced the average maximum scour depth by 28.2, 21.6, 18.5, and 20% at 12, 14, 16, and 18 l.s^{-1} flow rates, respectively. Increasing the flow rate was shown to intensify scour. By increasing Fr from 0.49 to 0.73, the maximum relative scour depth increased by 18%. Finally, a comparison between the physical model results and FLOW-3D simulations revealed a 3.4% difference between the simulation and experimental results. This comparison reveals how close the results are, proving the accuracy of the FLOW-3D simulation.

Declaration of competing interest

ACKNOWLEDGMENTS

REFERENCES

BOZKUS Z., ÇEŞME M. (2010). Reduction of scouring depth by using inclined piers, Canadian Journal of Civil Engineering, Vol. 37, Issue 12, pp. 1621-1630.

CHEREMISINOFF P.N., CHEREMISINOFF N.P., CHENG S.L. (1987). Cheng Hydraulic Mechanics 2, Civil Engineering Practice Technomic Publishing Company Inc., Lancaster, Pennsylvania, U.S.A.

CHIEW Y.M. (1992). Scour protection at bridge piers, Journal of Hydraulic Engineering, Vol. 118, Issue 9, pp. 1260-1269.

CHRETIES C., SIMARRO G., TEIXEIRA L. (2008). New Experimental Method to Find Equilibrium Scour at Bridge Piers, Journal of Hydraulic Engineering, pp. 1491-1495.

HASOUNIZADEH H. (1991). Investigating Prediction Methods for Local Scour Around Bridge Piers, Master, Shahid Chamran University of Ahwaz, Iran.

HIRT C.W., NICHOLS B.D. (1981). Volume of Fluid (VOF) Method for the Dynamics of Free Boundaries, Journal of Computational Physics, Vol. 39.

HOFFMANS G.J., VERHEIJ H.J. (1997). Scour manual, Vol. 96. CRC press.

KARIMI N., HEIDARNEJAD M., MASJEDI A. (2017). Scour depth at inclined bridge piers along a straight path: A laboratory study, Engineering science and technology, an International Journal, Vol. 20, Issue 4, pp. 1302-1307.

MELVILLE B. W., COLEMAN S.E. (2000). Bridge scour, Water Resources Publication.

NAJAFZADEH M., BARANI G.A., HESSAMI-KERMANI M.R. (2013a). Abutment scour in live-bed and clear-water using GMDH Network. Water Science and Technology, IWA, Vol. 67, Issue 5, pp. 1121-1128.

RICHARDSON E., DAVIES S. (1995). Evaluating scour at bridges, Rep. In Evaluating scour at bridges, Vol. 1, Federal Administration, USA.

WARDHANA K., HADIPRIONO F.C. (2003). Analysis of recent bridge failures in the United States, Journal of performance of constructed facilities, Vol. 17, Issue 3, pp. 144-150.